

Original Article

Optimized High Gain Interleaved Sepic Converter for Electric Vehicle Charging Stations with Emphasis on Renewable Energy Integration

R. Tamilmuthan¹, B.T. Geetha²

¹Department of Electrical and Electronics Engineering, Saveetha School of Engineering, SIMATS, Saveetha University, Tamilnadu, India.

²Department of Electronics and Communication Engineering, Saveetha School of Engineering, SIMATS, Saveetha University, Tamilnadu, India.

¹Corresponding Author : tamilamuthan.rdg@gmail.com

Received: 31 December 2023

Revised: 02 February 2024

Accepted: 01 March 2024

Published: 25 March 2024

Abstract - In the recent era, there has been a surge in the use of Electric Vehicles (EVs) as a result of rising fossil fuel prices and rising Carbon Dioxide (CO₂) emissions. Thus, an EV charging station that utilizes Renewable Energy Sources (RES) offers a significant advantage as well as a certain level of control. The fact that EV charging stations run on the current utility power grid systems places more strain on it and raises distribution-side load demands. As a consequence, this paper discusses the application of Photovoltaic (PV) fed energy efficient DC-DC high gain interleaved SEPIC converter with pigeon inspired optimization for ultra-fast charging systems. The proposed high-gain converter offers constant input current, capacity to handle the highest amount of current, increased efficacy and higher step-up voltage gain. Furthermore, the pigeon optimization algorithm is employed to regulate the high gain interleaved SEPIC converter that has an ability of rapid convergence speed and strong robustness with better optimization characteristics. The EV battery gets charged by the PV system, in scenarios of insufficient supply from PV system, the EV battery charges by extracting energy from the grid system. The overall proposed system is executed in MATLAB/Simulink. Finally, the comparative analysis is carried out to show the importance of developed work; as a result, the proposed high gain Interleaved SEPIC converter attains a high efficiency of 94.9% and low THD of 2.33% respectively.

Keywords - Electric Vehicle, High gain interleaved SEPIC converter, MATLAB/Simulink, Photovoltaic, Pigeon Inspired Optimization, Renewable Energy Sources.

1. Introduction

Over the past ten years, there has been a notable increase in the electrification of transport systems [1, 2]. This development is especially remarkable given its beneficial effects on the environment, as it helps reduce pollution, greenhouse gas emissions, and global warming. When distribution networks are electrified with renewable energy sources in conjunction with charging stations, intelligent grids can choose to reduce emissions and achieve high power conversion efficiency [3, 4].

The microgrid is made up of several dispersed energy sources as well as energy storage devices that are utilized locally by numerous kinds of loads and are either grid-connected or islanding [5]. Nonetheless, a high capacity penetration of EV charging stations drives up demand for the infrastructure necessary for charging, which in turn drives up demand for the utility grid [6]. One RES is solar (PV, which

is preferred for energy generation in many applications, particularly for electric vehicles [7].

Additionally, I-V and P-V curves of the PV system's electric nature exhibit non-linear behaviour that is dependent on temperature and the amount of sun insolation. However, because of the shadow effect, this approach is unable to produce a high and constant output voltage [8]. Using a DC-DC converter is one appropriate way to resolve this issue, which is possible to raise the output voltage of PV panels with high voltage gain [9, 10].

The low-voltage to high-voltage gain is increased by adopting a number of traditional DC-DC converters, including Boost [11], SEPIC [12], Cuk [13], Zeta [14], and Buck-Boost converters [15]. However, as previously indicated, converters have a unique set of issues; a traditional boost converter can function and increase low voltage [16].



Nevertheless, using high, extreme duty ratios causes typical boost converters' efficiency to decrease. Furthermore, the small number of inductors and capacitors in conventional converters makes them inappropriate for very high voltage gain. Furthermore, when the converter runs at a high extreme duty ratio, power MOSFET transistors are subjected to high voltage as well as high current stress [17, 18]. Furthermore, switching power losses dramatically rise when the converter operates at high voltage and a very high duty ratio. This also exacerbates the problem of reverse recovery because of diodes [19]. Hence, in this work, a novel high-gain interleaved SEPIC converter is implemented to overcome above stated issues, which has increased efficacy and higher voltage gain.

Additionally, the controller is needed to regulate the proposed DC-DC converter efficiently for various conventional controllers with optimization techniques like Fuzzy Logic Controllers [20], Artificial Neural Networks (ANN) [21], Particle Swarm Optimization (PSO) [22] and Grey Wolf Optimization (GWO) based PI controllers [23] are used to provide quick searches. Unfortunately, the increased computational demands of these techniques for stored data result in limitations on computational loading and handling that must be avoided [24].

In addition, the Firefly Algorithm (FA) offers excellent accuracy and a more straightforward implementation than the soft computing-based techniques [25]. Nonetheless, the main problems with the firefly technique are the appropriate parameter selection and increased computational complexity. Nonetheless, their slow convergence velocity is a significant drawback [26]. Therefore, the proposed work employed a pigeon-inspired optimization technique, which has the ability of rapid convergence speed and strong robustness with better optimization characteristics. The contributions of the proposed work are illustrated as follows.

- A novel high gain interleaved SEPIC converter for enhancing the output voltage from PV system with high efficiency.
- The pigeon-inspired optimization is employed to regulate the proposed converter, which has a high convergence speed.
- In scenarios of insufficient supply from PV system, the EV battery charges by extracting energy from the grid system.

2. Proposed Methodology

The electrification of transport systems has grown significantly over the past ten years, which is especially noteworthy given its beneficial effects on the environment as a result of its reduction of pollution, greenhouse gas emissions and global warming. Thus, an EV charging station utilizes RES, which offers a significant advantage as well as a certain level of control. As a consequence, this paper discusses the application of PV-fed high gain interleaved SEPIC converter with pigeon inspired optimization for ultra-fast charging systems. The block diagram for implemented work is represented in Figure 1, which is represented below.

The present research uses a novel high gain interleaved SEPIC converter to provide high voltage gain and efficiency by raising the low voltage from the PV system. By utilizing a pigeon-inspired optimization-based PI controller, the proposed converter gets efficiently controlled and can give better convergence speed with less settling time.

To create PWM pulses for the enhanced performance of the created converter, the regulated output is sent to the PWM generator. Delivered to the single-phase VSI, the regulated and consistent DC link voltage converts the DC-AC supply for voltage distribution to the grid system.

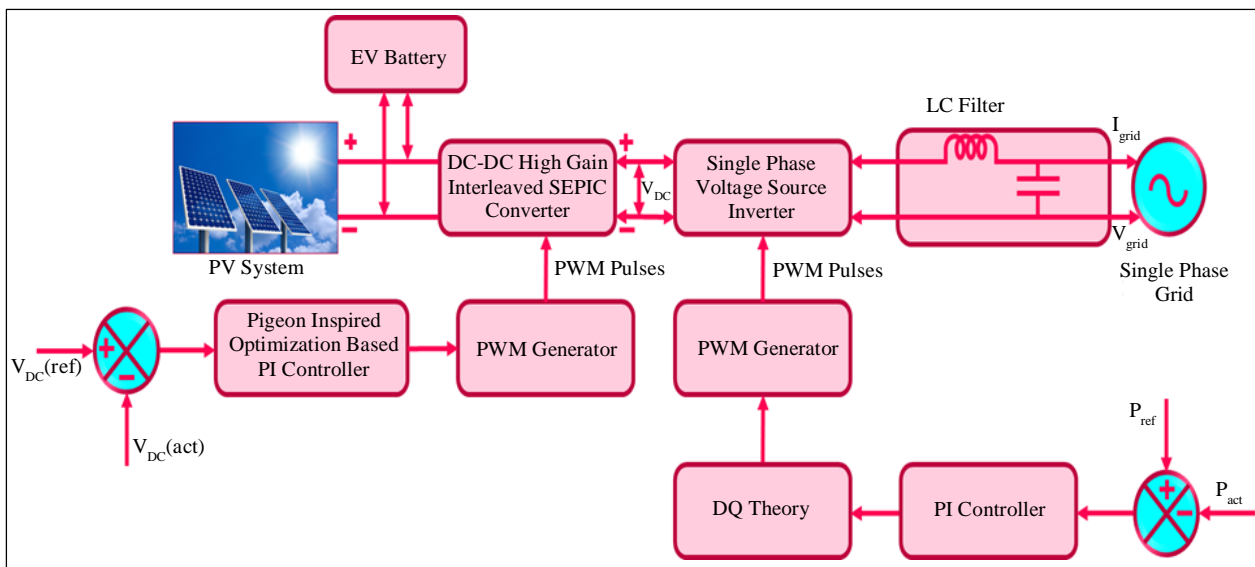


Fig. 1 Block diagram for the proposed framework

Actual power is compared with the reference power, which generates an error signal and is delivered to the PI controller for error compensation. The DQ theory compensates for the grid current distortion, and PWM pulses are produced by utilizing the PWM generator for better functioning of VSI. On the other hand, the EV battery gets charged by the PV system, in scenarios of insufficient supply from PV system, the EV battery charges by extracting energy from the grid system.

2.1. Modelling of PV System

In Figure 2, an equivalent circuit model represents an ideal PV system, and as illustrated in Figure 2, the fundamental current equation is as follows:

$$I = I_{pvcell} - I_{ocell} \left[\exp \frac{(qv)}{akT} - 1 \right] \tag{1}$$

$$I = I_{pv} - I_0 \left[e^{\frac{(v+R_s I)}{\alpha V_k}} - 1 \right] - \frac{(v+R_s I)}{R_p} \tag{2}$$

Where, V_k represents thermal voltage, q specifies the electron charge, I_{pv} denotes the photocurrent, T shows the cell's temperature, α illustrates the ideality factor, R_s represents the series resistance, I_0 indicates the cell saturation of dark current and R_p shunt resistance, respectively. The

number of arrays in the PV panel, temperature, and radiation all affect the PV current. Equation 2 thus turns into,

$$I = I_{pv} - I_0 \left[\exp \frac{(v+R_s I)q}{\alpha kT.N_s} - 1 \right] - \frac{(v+R_s I)}{R_p} \tag{3}$$

Here, N_s denotes to the series of connected cells. Hence, a novel high gain interleaved SEPIC converter is utilized to boost low voltage obtained from the PV system, which is described as follows.

2.2. Modelling of High Gain Interleaved SEPIC Converter

This study presents a novel high-gain SEPIC structure for high-voltage applications, depicted in Figure 3. Depending on the PWM pulse's duty ratio, the developed high-gain interleaved SEPIC converter exhibits a great degree of flexibility in operating in both boost and buck modes. The developed converter contains four diodes (D_1, D_2, D_3, D_4), four capacitors (C_1, C_2, C_3, C_4), six inductors ($L_1, L_2, L_3, L_4, L_5, L_6$) and two switches S_1 and S_2 respectively.

The implemented converter's salient characteristics are as follows: it takes continuous input current, it has a high voltage gain, and it maximizes the use of the input source. Figure 4 illustrates the four modes of operation for the non-isolated DC-DC.

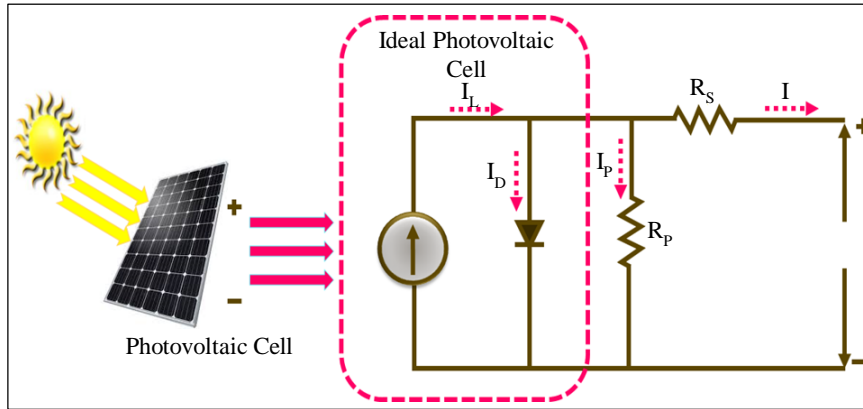


Fig. 2 Circuit of PV system

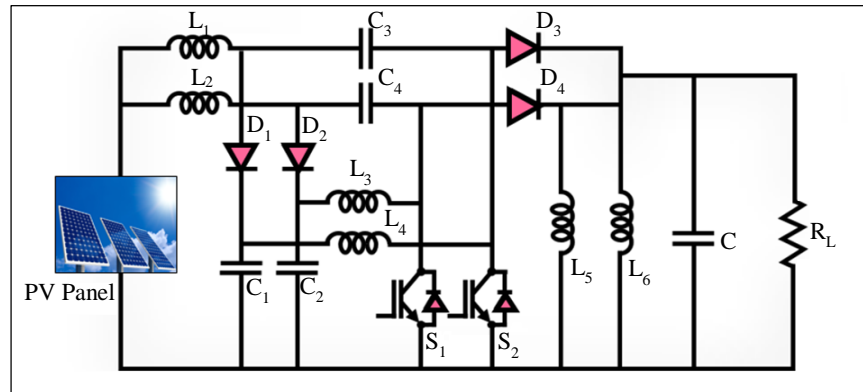


Fig. 3 Circuit of high gain interleaved SEPIC converter

2.2.1. Analysis of the Proposed High-Gain Converter

During steady state for the inductor L_1 ,

$$V_i(t_{on} + t_{off}) = V_{cm}t_{off} \quad (4)$$

$$V_i(DT + (1 - D)T) = V_C(1 - D)T \quad (5)$$

$$V_iT = V_C(1 - D)T \quad (6)$$

V_C capacitor voltage is defined by Equation 7, which is found in traditional boost converters,

$$V_C/V_i = V_i/1 - D \quad (7)$$

During the switch in the OFF state, the diodes are in conduction states,

$$V_0 = V_{CS} + V_C \quad (8)$$

$$V_{CS} = V_0 - V_C \quad (9)$$

When the inductor is in a stable condition, its average voltage is zero.

$$(V_C - V_{CS})T_{on} = (V_0 - V_C)T_{off} \quad (10)$$

$$(V_C - V_{CS})D = (V_0 - V_C)(1 - D) \quad (11)$$

From Equations 7, 9, and 10 the static gain of the proposed converter.

$$(V_C - (V_0 - V_C))T_{on} = (V_0 - V_C)T_{off} \quad (12)$$

$$(2V_C t_{on} + V_C t_{off}) = V_0 t_{off} + V_0 t_{on} \quad (13)$$

$$V_C(DT + T) = V_0T \quad (14)$$

$$V_0/V_i = D + 1/D - 1 \quad (15)$$

The voltage of the series capacitor V_{CS} is defined by substituting Equations 7 & 15 in Equation 11, thus

$$V_{CS}/V_i = D/1 - D \quad (16)$$

Mode 1

In mode 1, S_2 switch is ON state and S_1 switch is OFF state in this mode. Capacitors C_1, C_2, C_3, C_4 receive a charge from the PV output potential, while inductors L_1, L_2, L_3 , are discharged by the load. Whereas the diode D_2, D_3 stops the return current from load and D_1, D_4 becomes forward-biased and supplies the current to the load system.

Mode 2

In this mode, switch S_1 is closed while switch S_2 is open. While the inductors L_1, L_2, L_4 discharge the energies over the load, the inductors L_3, L_5, L_6 get a charge from the input PV source. In this mode, the PV system's return current is blocked by the diode D_1, D_4 .

Mode 3

S_1 and S_2 switches are in OFF condition in Mode 3. In this mode, the load causes the inductors to L_1, L_2, L_3, L_4, L_5 and L_6 to discharge. D_1, D_2, D_3, D_4 Diodes exhibit forward bias.

Mode 4

The switches S_1 and S_2 are in the ON state during this mode, together with D_1, D_2 in ON state. The input PV charges the inductors L_1, L_2, L_3, L_4, L_5 and L_6 during this period. Because the diodes are in reverse bias, diodes D_3, D_4 block the current from the load due to the reverse bias condition.

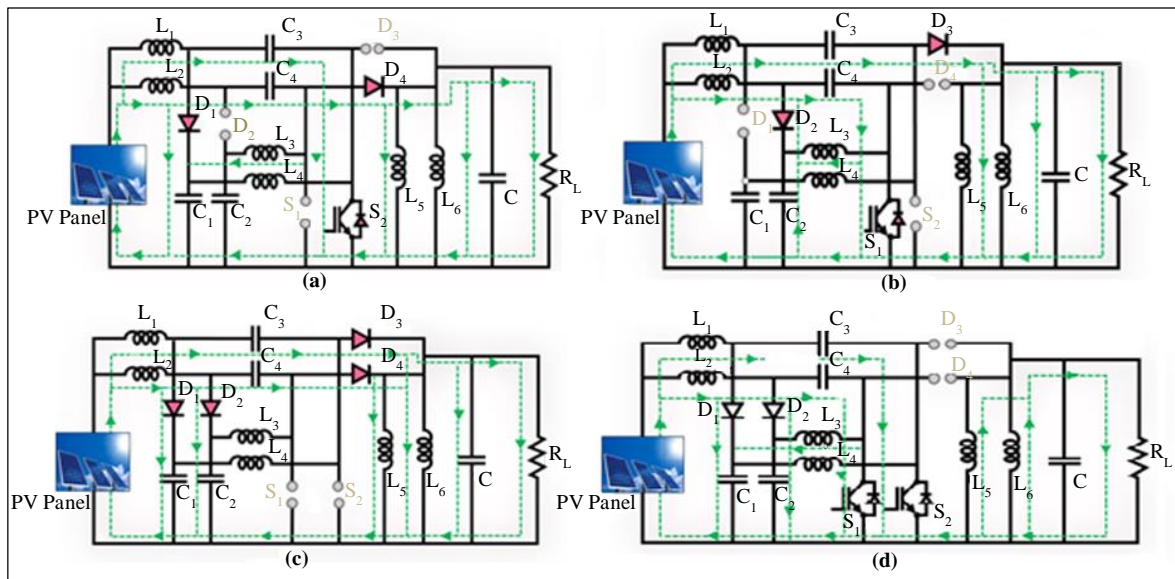


Fig. 4 Modes of operation (a) Mode 1, (b) Mode 2, (c) Mode 3, and (d) Mode 4.

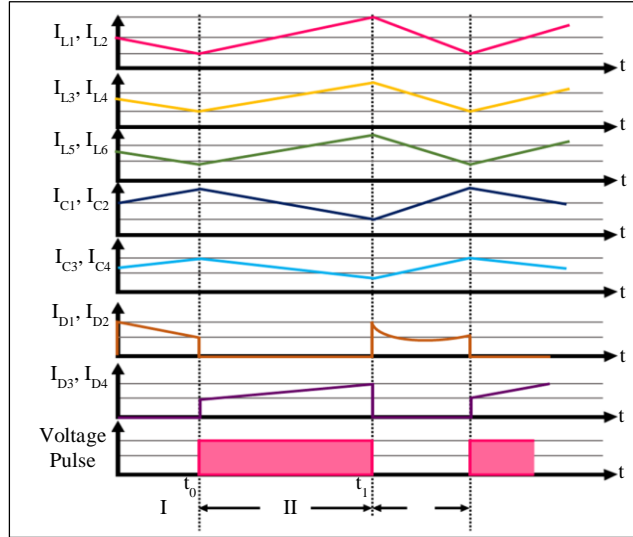


Fig. 5 Waveform for proposed high gain converter

By adopting the developed high gain converter, the voltage gets boosted with high efficiency and decreased switching losses. To regulate the developed converter, a pigeon-inspired optimization technique is utilized that is illustrated as follows.

2.3. Modelling of Pigeon-Inspired Optimization

“Pigeon” is a word that comes from the Latin word “pipio,” which means “young cheeping bird.” One ubiquitous and well-liked species of bird is the pigeon. There are two

types of pigeons: the wild one lives along the coast, and the feral one lives almost entirely in places where people live.

Due to their homing instinct, pigeons were formerly employed by the military. The PIO is a revolutionary population-based optimization system, and it is based on the natural behaviour of pigeons, which consistently and reliably find their destination. The following guidelines are used to construct two operators that idealize certain pigeon-homing characteristics:

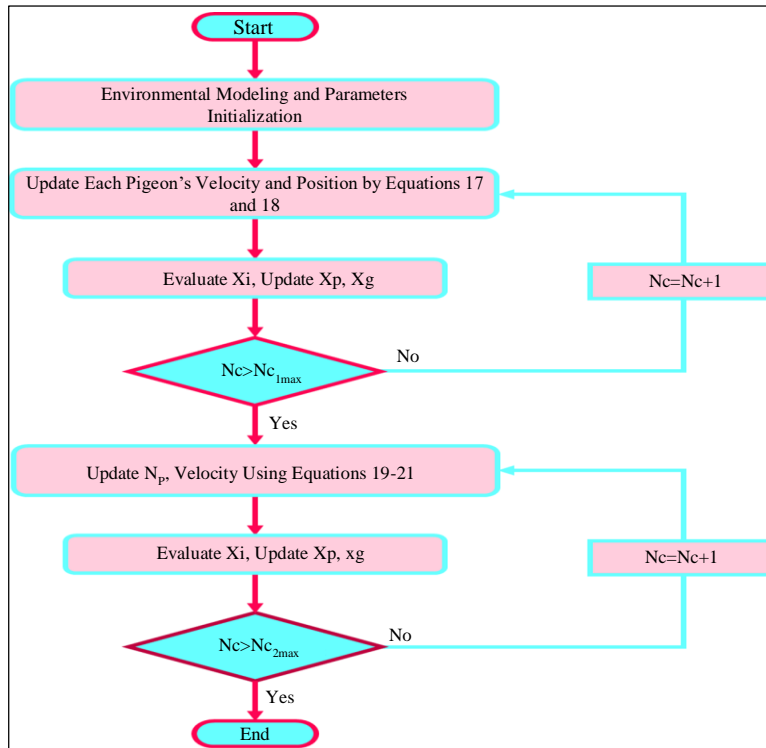


Fig. 6 Flowchart of the pigeon-inspired algorithm

2.3.1. Map and Compass Operator

Virtual pigeons are utilized naturally in the PIO model. The position X_i and velocity V_i of pigeon i are used to construct the rules in this map and compass operator, and each iteration updates the positions as well as velocities in a D dimension search space. Pigeon's new position X_i and velocity V_i at t -th iteration used to determine by the following formulas,

$$V_i(t) = V_i(t-1) \cdot e^{-Rt} + rand. (X_g - X_i(t-1)) \quad (17)$$

$$X_i(t) = X_i(t-1) + V_i(t) \quad (18)$$

Where X_g denotes the current global best position that is found by comparing all of the pigeons' positions, R specifies map and compass factor, and $rand$ specifies a random number. Equation 17, represented by the thick arrows, allows each pigeon to modify its flying direction by tracking this particular pigeon.

Equation 17 relates. $V_i(t-1) \cdot e^{-Rt}$ to thin arrows, which represent the previous flying direction. The direction it will fly in next is indicated by the vector sum of these two arrows.

2.3.2. Landmark Operator

Each generation, the landmark operator reduces the pigeon population by half. The pigeons are not familiar with the sights and are still a long way from their destination. Assume that every pigeon can fly directly to the target and that. $X_c(t)$ is the centre of approximately the pigeon's position at the t -th iteration.

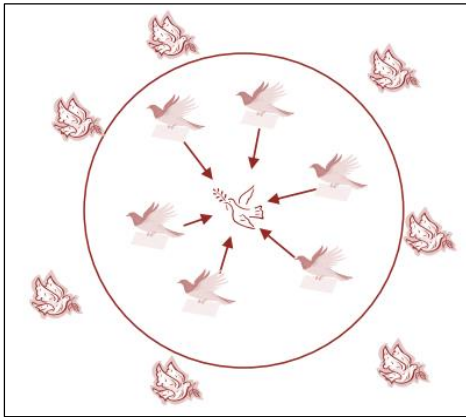


Fig. 7 Landmark operator of PIO

At the t -th iteration, the position update rule for Pigeon i is as follows:

$$N_p(t) = \frac{N_p(t-1)}{2} \quad (19)$$

$$X_c(t) = \frac{\sum X_i(t) \cdot fitness(X_i(t))}{N_p \sum fitness(X_i(t))} \quad (20)$$

$$X_i(t) = X_i(t-1) + rand. X_c(t) - X_i(t-1) \quad (21)$$

Where the pigeon's particular quality is denoted by fitness (f), one possible option for the minimum optimization issues is to select a fitness. $X_i(t) = \frac{1}{f_{\min}(X_i(t)+\epsilon)}$. This can select fitness $X_i(t) = f_{\max} X_i(t)$ for maximum optimization problems. The ideal location of the N_c -th iteration for each individual pigeon is indicated by X_p and $X_p = \min X_{i1}, X_{i2}, \dots, X_{iNc}$.

The implemented PIO optimization algorithm provides a better settling time with the greatest convergence speed. Moreover, the DQ theory for producing the reference current is explained in the section that follows.

2.4. Modelling of DQ Theory for Reference Current Generation

The method of extracting synchronous harmonic dq frame current is useful for selecting harmonic frequencies that require compensation, but it comes with a higher computational cost. Finding the basic load current component and using it to identify the additional non-active current component that causes harmonics and reactive power, as stated in (22), is a more simple method.

$$i_{na}(t) = i_i(t) - i_a(t) \quad (22)$$

The real power consumed by non-linear load $i_{na}(t)$ is attributed to the active component. In this sense, even if it comes with a higher power rating, the APF makes the most of everything. The d-q transformation is inherently designed for single-phase systems, in which the instantaneous active and reactive power components are initially transformed into two orthogonal components. The d-q transformation, sometimes referred to as Park Transformation, is produced if these orthogonal components are rotated at the vital frequency of the source voltage. Figure 2 illustrates the resulting harmonic extraction process. Phase Locked Loop subsystem can provide the necessary synchronizing signal for transformation. The reference currents are acquired once the coordinates are converted from $\alpha\beta$ to ABC coordinates.

$$\begin{bmatrix} i^*_a \\ i^*_b \\ i^*_c \end{bmatrix} = \sqrt{\frac{2}{3}} \begin{bmatrix} 1 & 0 \\ -\frac{1}{2} & \frac{\sqrt{3}}{2} \\ -\frac{1}{2} & -\frac{\sqrt{3}}{2} \end{bmatrix} \begin{bmatrix} i^*_{\alpha} \\ i^*_{\beta} \end{bmatrix} \quad (23)$$

Convert the ABC coordinate system to a stationary (α - β) reference frame using Clarke's Transformation.

$$\begin{bmatrix} x_{\alpha} \\ x_{\beta} \end{bmatrix} = \sqrt{\frac{2}{3}} \begin{bmatrix} 1 & -\frac{1}{2} & -\frac{1}{2} \\ 0 & \frac{\sqrt{3}}{2} & -\frac{\sqrt{3}}{2} \end{bmatrix} \begin{bmatrix} x_a \\ x_b \\ x_c \end{bmatrix} \quad (24)$$

In this case, the variable under consideration, voltage or current, is denoted by x .

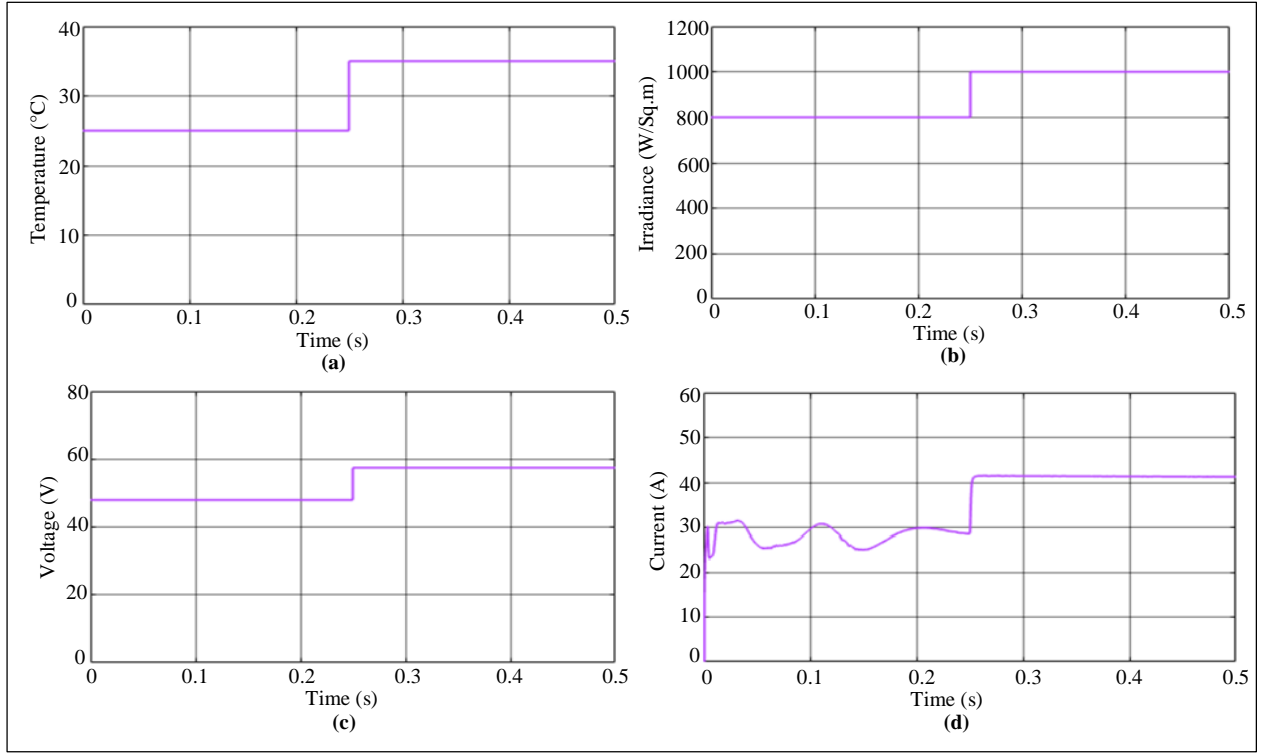


Fig. 9 Solar panel waveform on case 1 (a) Temperature, (b) Irradiance, (c) Voltage, and (d) Current.

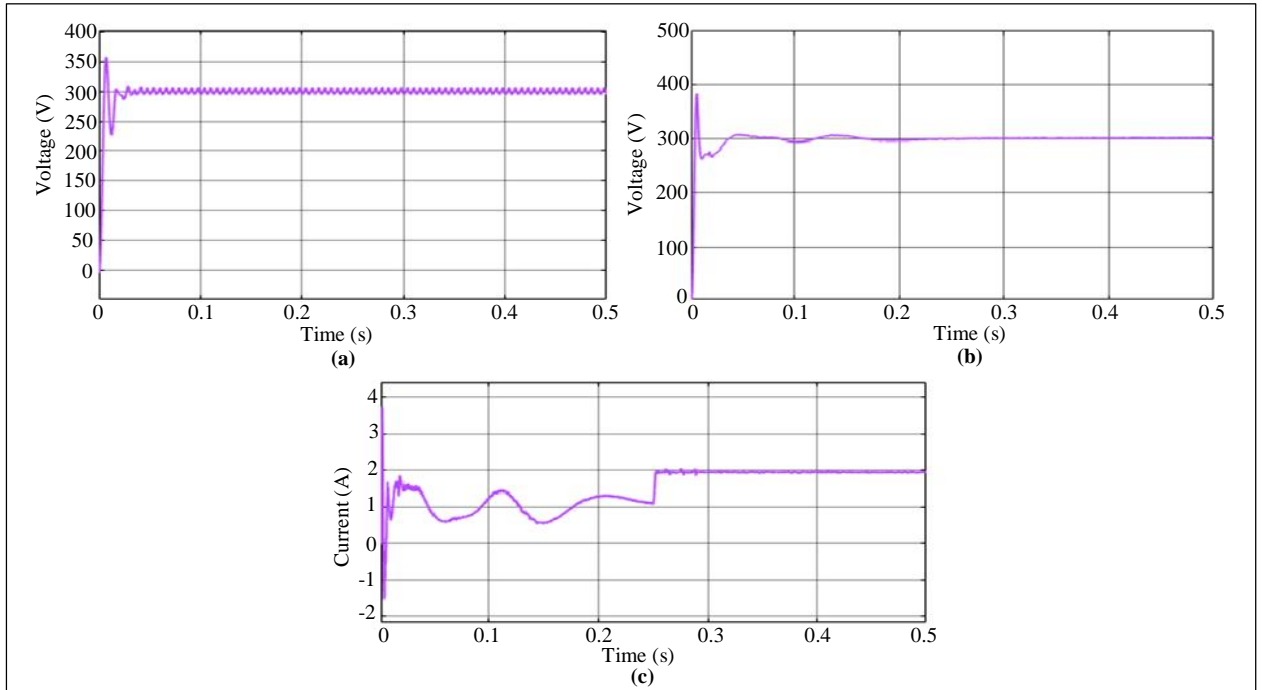


Fig. 10 Waveform for a converter on case 1 (a) Voltage using PI controller, (b) Voltage using optimized PI controller, and (c) Output current.

The converter waveform is represented in Figure for case 1, from Figure 10(a), the output voltage waveform utilizing the PI controller fluctuated high during the initial period, and it slightly maintained constant with distortions. To maintain constant voltage without any distortion, the pigeon-inspired

optimized PI controller is utilized as specified in Figure 10(b); after that, the constant output voltage is attained at 300V after 0.3s. Moreover, the current is highly raised and varied initially after 0.35s; it is constantly maintained at 2A, as shown in Figure 10(c).

3.2. Case 2: Varying Solar Panel Temperature Constant Irradiance

The solar panel waveform for case 2 is represented in Figure 11. Figure 11(a) shows the temperature waveform, which indicates that the temperature fluctuates at first; after 0.25s it maintained constant at 35V. Likewise, the irradiance

of the solar panel is continuously upheld at 1000 W/Sq.m. Moreover, the voltage oscillated slightly in the initial time; after 0.25s, it maintained constant at 59V as specified in Figure 11(c). As denoted in Figure 11(d), initially, the current gets highly raised and fluctuates certain period of time; after 0.25s, the current upheld constant at 42A correspondingly.

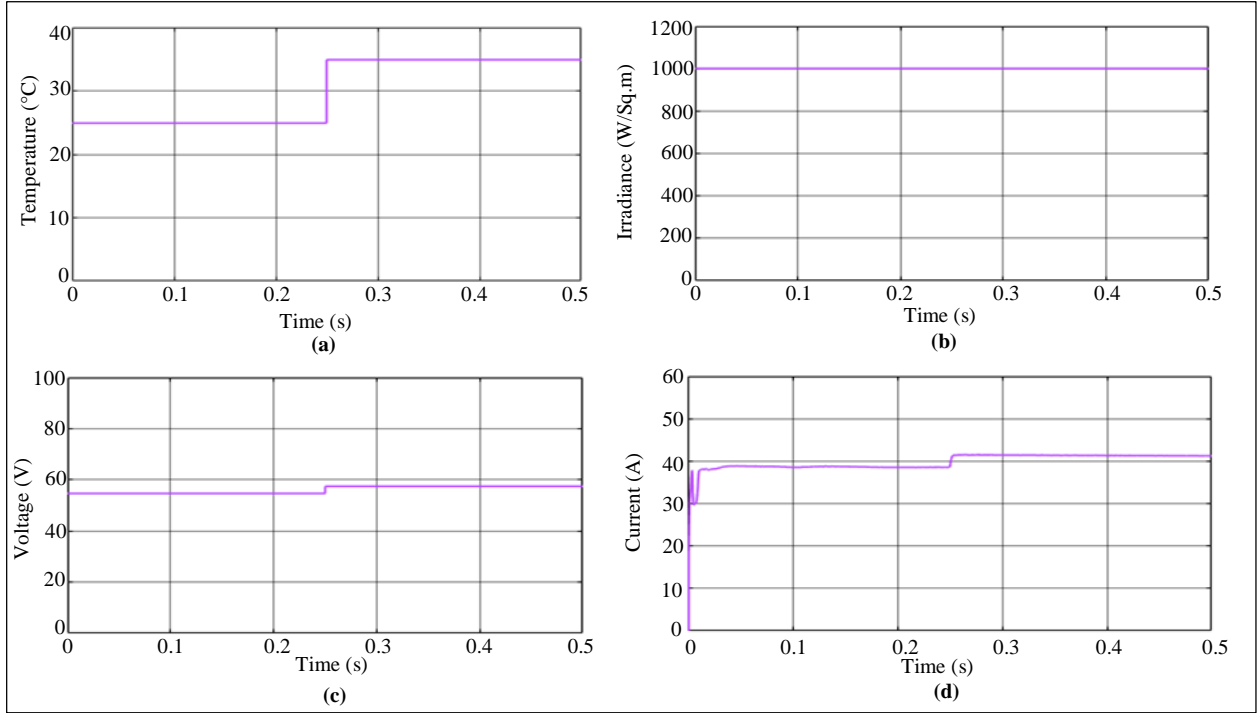


Fig. 11 Solar panel waveform on case 2 (a) Temperature, (b) Irradiance, (c) Voltage, and (d) Current.

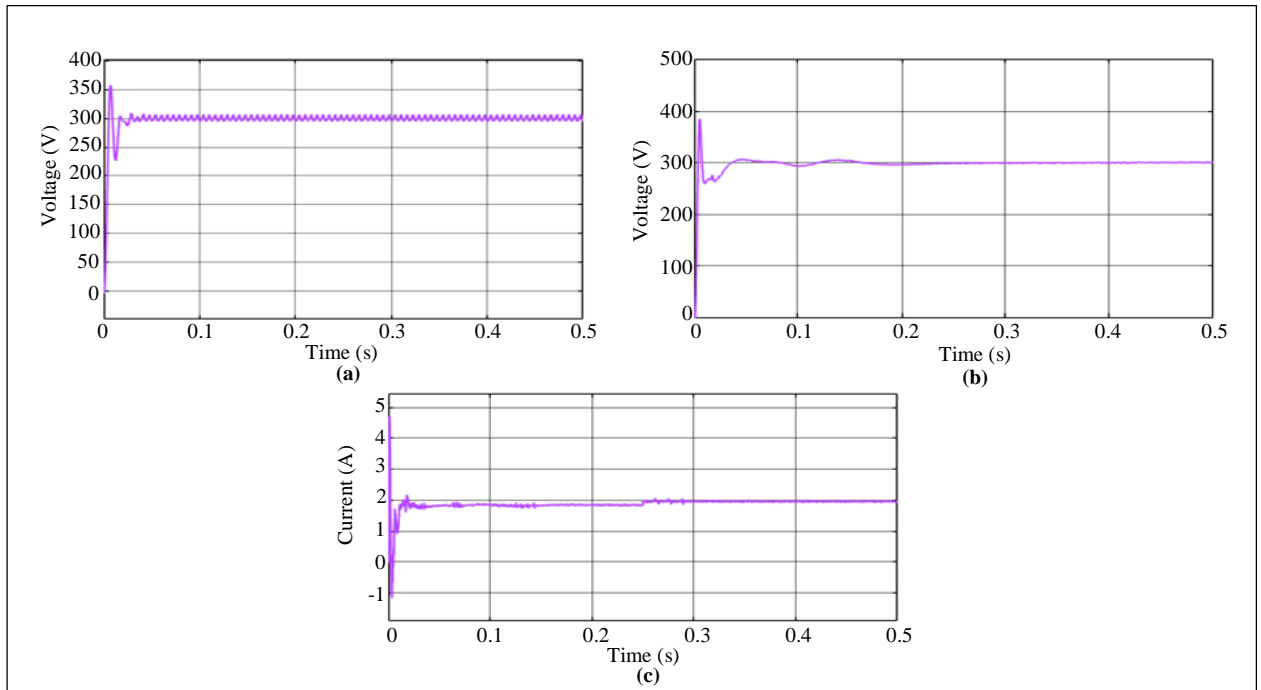


Fig. 12 Waveform for converter on case 2 (a) Voltage using PI controller, (b) Voltage using optimized PI controller, and (c) Output current.

Figure 12 specifies the proposed converter waveform for case 2; the output voltage waveform using the PI controller gets highly fluctuated and is maintained with slight distortion, as demonstrated in Figure 12(a). Similarly, as represented in Figure 12(b) converter output voltage utilizing proposed

pigeon inspired optimization, the constant voltage is attained after 0.3s. Furthermore, the current output waveform for the developed converter is specified in Figure 12(c), which is analyzed that initially the current oscillated and it constantly upheld at 2A after 0.4s respectively.

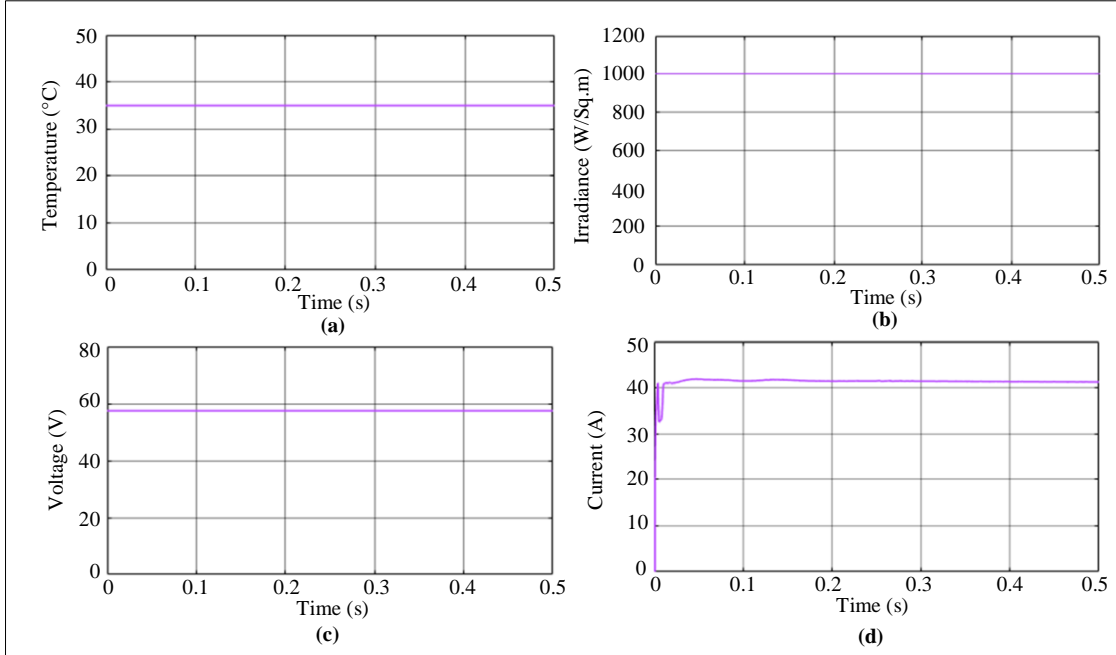


Fig. 13 Solar panel waveform on case 3 (a) Temperature, (b) Irradiance, (c) Voltage, and (d) Current.

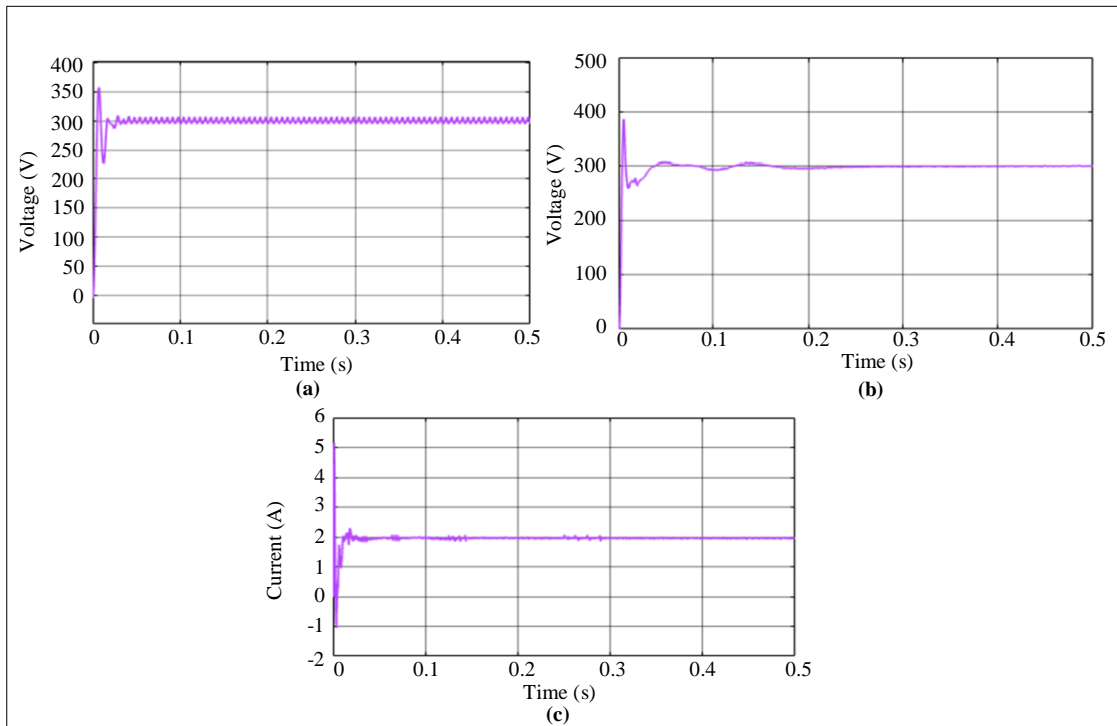


Fig. 14 Waveform for converter on case 3 (a) Voltage using PI controller, (b) Voltage using optimized PI controller, and (c) output current.

3.3. Case 3: Constant Solar Panel Temperature and Irradiance

Figure 13 illustrates the solar panel waveform for case 3, which is analyzed as shown in Figure 13(a), the temperature gets continually upheld at 35C. Similarly, the irradiance is constantly maintained at 1000(W/Sq.m), as specified in Figure 13(b). Furthermore, solar panel voltage is preserved constant at 58V. The current for the solar panel fluctuated slightly and it gradually kept at 42A after 0.3s respectively.

Figure 14 specifies the proposed converter waveform for case 3, as demonstrated in Figure 14(a), the output voltage waveform utilizing the PI controller gets highly fluctuated with distortion. Likewise, the converter output voltage utilizing the proposed pigeon inspired optimization for case 3, the constant voltage is upheld at 300V after 0.3s. Moreover, the current output waveform for the developed converter is specified in Figure 14(c), which is analyzed that initially, the current oscillated and it continuously upheld at 2A after 0.35s.

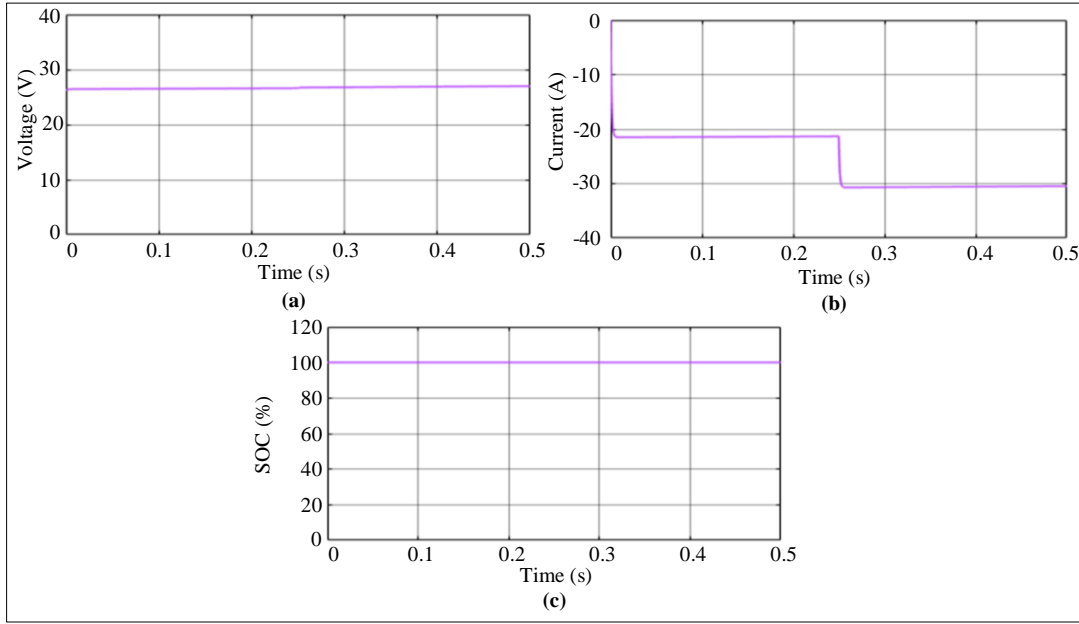


Fig. 15 Waveform for Battery (a) Voltage, (b) Current, and (c) SOC.

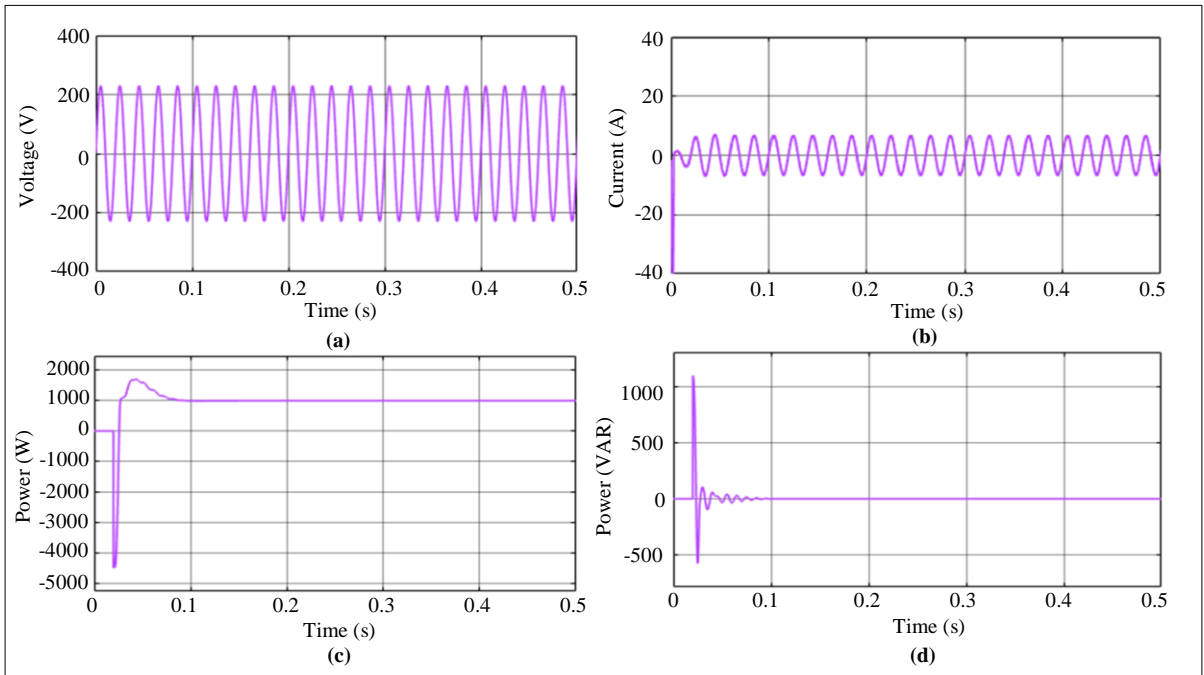


Fig. 16 Waveform for (a) Grid voltage, (b) Grid Current, (c) Real power, and (d) Reactive power.

The waveform for the battery is demonstrated in Figure 15; the battery voltage is maintained its constant voltage at 27V as denoted in Figure 15(a).

Furthermore, the current initially oscillated during a specific period and after 0.25s, the current was constantly maintained at -29A as represented in Figure 15(b), and the state of charge in the battery is 100% as specified in Figure 15(c) respectively. The Waveform for Grid voltage, grid Current, Real power as well as Reactive power is illustrated in Figure 16; the grid voltage waveform specified in Figure 16(a) states that voltage is constantly maintained at 220 to-220.

Similarly, the grid current is maintained constant at 10 to 10A, as illustrated in Figure 16(b). Figures 16(c) and 16(d)

represent that the stable real and reactive power is accomplished with an improved unity power factor. The THD waveform for the proposed high gain converter is signified in Figure 17, which shows that the developed converter has a 2.33% THD value, respectively.

Figure 18 represents the comparison of converters for Efficiency and THD; from graph 18(a) and Table 2, it is analyzed that the developed converter has a higher efficiency of 94.9% than existing converters like Boost, Buck-Boost, and interleaved SEPIC.

In a similar vein, as shown in Figure 18(b), the THD value for the implemented converter achieves a lower THD value of 2.33% in comparison to the topologies now in use.

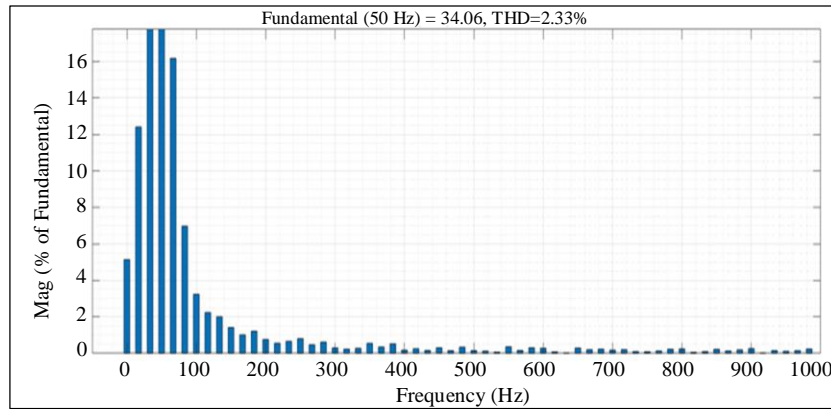


Fig. 17 THD waveform

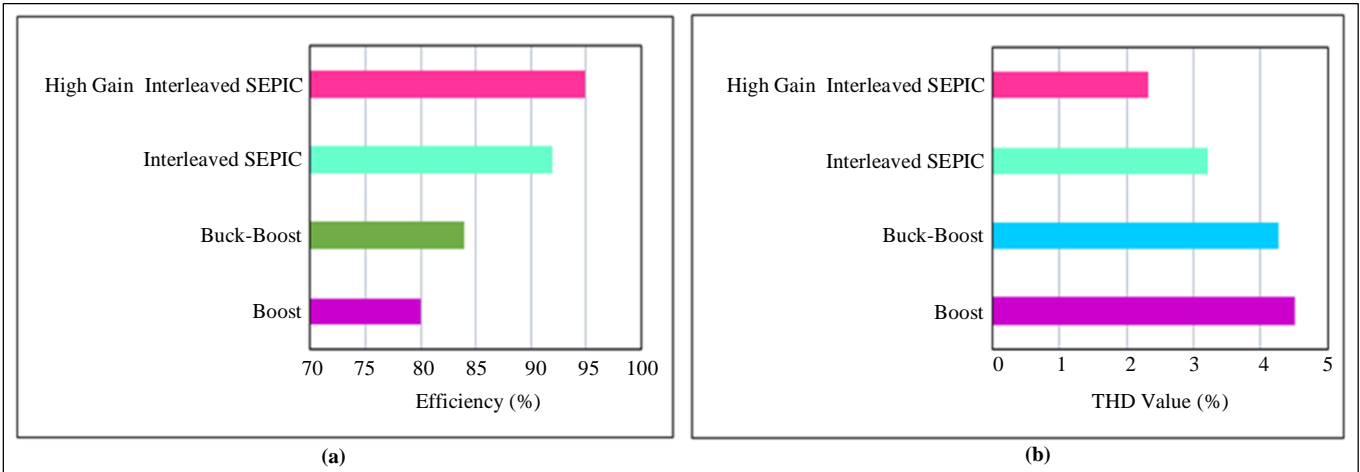


Fig. 18 Comparison of Converters for (a) Efficiency, and (b) THD value.

Table 2. Comparison of efficiency

Converters	Efficiency (%)
Boost [27]	80
Buck-Boost [28]	84
Interleaved SEPIC [29]	92
Proposed Converter	94.9

Comparison of optimized controllers like PSO and ABC-based PI controllers with the proposed pigeon-inspired optimized PI controller as illustrated in Table 3, which is observed that the developed, optimized controller has less settling time and rise time by the value of 0.3s and 0.01s compared to the conventional techniques.

Table 3. Comparison of optimized controller

Controllers	Settling time (s)	Rise time (s)
PSO Optimized PID [30]	9.7825	0.5783
ABC Optimized PID [31]	5.57	0.261
Proposed	0.3	0.01

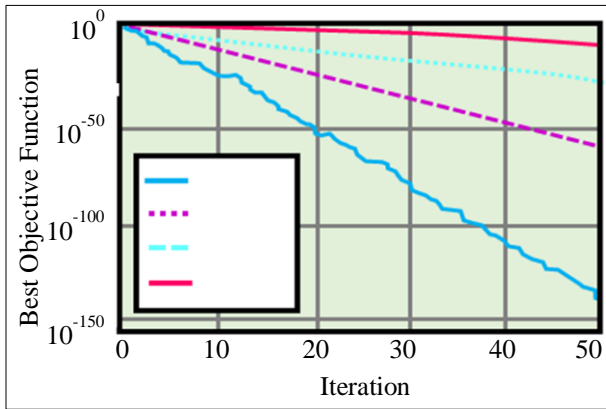


Fig. 19 Comparison of convergence speed

The convergence speed for the proposed pigeon-inspired optimization is compared with the conventional topologies like PSO, ABC, and FFA, as illustrated in Figure 19, which shows that compared to existing techniques, the developed optimization method attains rapid convergence speed.

4. Conclusion

This research presents the application of energy-efficient high-power PV fed interleaved high-gain DC-DC converter with pigeon-inspired optimization for ultra-fast charging systems. Constant input current, enhanced efficacy, high voltage gain and higher quality DC voltage generation are attained by the developed novel high gain converter.

Additionally, the high-gain proposed converter is efficiently controlled by the pigeon optimization method, which provides improved optimization features, strong robustness and speedy convergence speed. When the PV system is unable to provide enough energy due to the ecological changes, the EV battery is charged by extracting energy from the grid system.

The entire suggested system is run in MATLAB/Simulink, and a comparative analysis is conducted to validate the significance of the generated work. As a consequence, the better efficiency of 94.9% and reduced THD of 2.33% are achieved using interleaved SEPIC converters as well as less settling time of 0.3s is attained by adopting the proposed pigeon-inspired optimization algorithm, respectively.

References

- [1] K.S. Kavin, and P. Subha Karuvelam, "PV-Based Grid Interactive PMBLDC Electric Vehicle with High Gain Interleaved DC-DC SEPIC Converter," *IETE Journal of Research*, vol. 69, no. 7, pp. 4791-4805, 2023. [CrossRef] [Google Scholar] [Publisher Link]
- [2] Christian Breyer et al., "On the History and Future of 100% Renewable Energy Systems Research," *IEEE Access*, vol. 10, pp. 78176-78218, 2022. [CrossRef] [Google Scholar] [Publisher Link]
- [3] Krystian Pietrzak, and Oliwia Pietrzak, "Environmental Effects of Electromobility in a Sustainable Urban Public Transport," *Sustainability*, vol. 12, no. 3, pp. 1-21, 2020. [CrossRef] [Google Scholar] [Publisher Link]
- [4] G. Sree Lakshmi et al., "Electric Vehicles Integration with Renewable Energy Sources and Smart Grids," *Advances in Smart Grid Technology*, pp. 397-411, 2020. [CrossRef] [Google Scholar] [Publisher Link]
- [5] Glen G. Farivar et al., "Grid-Connected Energy Storage Systems: State-of-the-Art and Emerging Technologies," *Proceedings of the IEEE*, vol. 11, no. 4, pp. 397-420, 2023. [CrossRef] [Google Scholar] [Publisher Link]
- [6] Zhijie Lai, and Sen Li, "On-Demand Valet Charging for Electric Vehicles: Economic Equilibrium, Infrastructure Planning and Regulatory Incentives," *Transportation Research Part C: Emerging Technologies*, vol. 140, 2022. [CrossRef] [Google Scholar] [Publisher Link]
- [7] Masafumi Yamaguchi et al., "Development of High-Efficiency and Low-Cost Solar Cells for PV-Powered Vehicles Application," *Progress in Photovoltaics: Research and Applications*, vol. 29, no. 7, pp. 684-693, 2021. [CrossRef] [Google Scholar] [Publisher Link]
- [8] Piero Bevilacqua et al., "An Accurate Thermal Model for the PV Electric Generation Prediction: Long-Term Validation in Different Climatic Conditions," *Renewable Energy*, vol. 163, pp. 1092-1112, 2021. [CrossRef] [Google Scholar] [Publisher Link]
- [9] R. Ragul et al., "PV Based Standalone DC-Micro Grid System for EV Charging Station with New GWO-ANFIS MPPTs under Partial Shading Conditions," *International Transactions on Electrical Energy Systems*, vol. 2023, pp. 1-14, 2023. [CrossRef] [Google Scholar] [Publisher Link]
- [10] V. Fernão Pires et al., "Dual Output and High Voltage Gain DC-DC Converter for PV and Fuel Cell Generators Connected to DC Bipolar Microgrids," *IEEE Access*, vol. 9, pp. 157124-157133, 2021. [CrossRef] [Google Scholar] [Publisher Link]

- [11] Konstantinos Zaoskoufis, and Emmanuel C. Tatakis, "An Improved Boost-Based DC/DC Converter with High-Voltage Step-Up Ratio for DC Microgrids," *IEEE Journal of Emerging and Selected Topics in Power Electronics*, vol. 9, no. 2, pp. 1837-1853, 2021. [[CrossRef](#)] [[Google Scholar](#)] [[Publisher Link](#)]
- [12] Sara Hasanpour et al., "A New High-Gain, High-Efficiency SEPIC-Based DC-DC Converter for Renewable Energy Applications," *IEEE Journal of Emerging and Selected Topics in Industrial Electronics*, vol. 2, no. 4, pp. 567-578, 2021. [[CrossRef](#)] [[Google Scholar](#)] [[Publisher Link](#)]
- [13] Binxin Zhu et al., "Single-Switch High Step-Up Zeta Converter Based on Coat Circuit," *IEEE Access*, vol. 9, pp. 5166-5176, 2020. [[CrossRef](#)] [[Google Scholar](#)] [[Publisher Link](#)]
- [14] Zeeshan Haider et al., "Development and Analysis of a Novel High-Gain CUK Converter Using Voltage-Multiplier Units," *Electronics*, vol. 11, no. 17, pp. 1-16, 2022. [[CrossRef](#)] [[Google Scholar](#)] [[Publisher Link](#)]
- [15] Binxin Zhu et al., "Low-Voltage Stress Buck-Boost Converter with a High-Voltage Conversion Gain," *IEEE Access*, vol. 8, pp. 95188-95196, 2020. [[CrossRef](#)] [[Google Scholar](#)] [[Publisher Link](#)]
- [16] Anurag Priyadarshi, Pratik Kumar Kar, and Srinivas Bhaskar Karanki, "A Wide Load Range ZVS High Voltage Gain Hybrid DC-DC Boost Converter Based on Diode-Capacitor Voltage Multiplier Circuit," *International Transactions on Electrical Energy Systems*, vol. 30, no. 1, 2020. [[CrossRef](#)] [[Google Scholar](#)] [[Publisher Link](#)]
- [17] Javed Ahmad et al., "A New High-Gain DC-DC Converter with Continuous Input Current for DC Microgrid Applications," *Energies*, vol. 14, no. 9, pp. 1-14, 2021. [[CrossRef](#)] [[Google Scholar](#)] [[Publisher Link](#)]
- [18] Nagaraju Addagatla, and Rajender Boini, "A High Gain Single Switch DC-DC Converter with Double Voltage Booster Switched Inductors," *Advances in Science and Technology Research Journal*, vol. 17, no. 2, pp. 1-11, 2023. [[CrossRef](#)] [[Google Scholar](#)] [[Publisher Link](#)]
- [19] Koteswara Rao Kothapalli et al., "Soft-Switched Ultrahigh Gain DC-DC Converter with Voltage Multiplier Cell for DC Microgrid," *IEEE Transactions on Industrial Electronics*, vol. 68, no. 11, pp. 11063-11075, 2020. [[CrossRef](#)] [[Google Scholar](#)] [[Publisher Link](#)]
- [20] Younes Boujoudar et al., "Fuzzy Logic-Based Controller of the Bidirectional Direct Current to Direct Current Converter in Microgrid," *International Journal of Electrical and Computer Engineering (IJECE)*, vol. 13, no. 5, pp. 4789-4797, 2023. [[CrossRef](#)] [[Google Scholar](#)] [[Publisher Link](#)]
- [21] Daming Wang et al., "Model Predictive Control Using Artificial Neural Network for Power Converters," *IEEE Transactions on Industrial Electronics*, vol. 69, no. 4, pp. 3689-3699, 2022. [[CrossRef](#)] [[Google Scholar](#)] [[Publisher Link](#)]
- [22] Shaharyar Yousaf et al., "A Comparative Analysis of Various Controller Techniques for Optimal Control of Smart Nano-Grid Using GA and PSO Algorithms," *IEEE Access*, vol. 8, pp. 205696-205711, 2020. [[CrossRef](#)] [[Google Scholar](#)] [[Publisher Link](#)]
- [23] Jesus Aguila-Leon et al., "Solar Photovoltaic Maximum Power Point Tracking Controller Optimization Using Grey Wolf Optimizer: A Performance Comparison between Bio-Inspired and Traditional Algorithms," *Expert Systems with Applications*, vol. 211, 2023. [[CrossRef](#)] [[Google Scholar](#)] [[Publisher Link](#)]
- [24] A. Francis Saviour Devaraj et al., "Hybridization of Firefly and Improved Multi-Objective Particle Swarm Optimization Algorithm for Energy Efficient Load Balancing in Cloud Computing Environments," *Journal of Parallel and Distributed Computing*, vol. 142, pp. 36-45, 2020. [[CrossRef](#)] [[Google Scholar](#)] [[Publisher Link](#)]
- [25] Mohsen Zare et al., "A Global Best-Guided Firefly Algorithm for Engineering Problems," *Journal of Bionic Engineering*, vol. 20, pp. 2359-2388, 2023. [[CrossRef](#)] [[Google Scholar](#)] [[Publisher Link](#)]
- [26] Jinran Wu et al., "An Improved Firefly Algorithm for Global Continuous Optimization Problems," *Expert Systems with Applications*, vol. 149, 2020. [[CrossRef](#)] [[Google Scholar](#)] [[Publisher Link](#)]
- [27] Nabil Aouchabana et al., "Power Efficiency Improvement of a Boost Converter Using a Coupled Inductor with a Fuzzy Logic Controller: Application to a Photovoltaic System," *Applied Sciences*, vol. 11, no. 3, pp. 1-19, 2021. [[CrossRef](#)] [[Google Scholar](#)] [[Publisher Link](#)]
- [28] R. Abhishek, Pallavi Zoting, and Purva Ragit, "Design and Analysis of a DC-DC Buck Converter and Boost Converter to Achieve High Efficiency by Altering Duty Cycle and Input Voltage," *International Journal of Scientific and Research Publications*, vol. 10, no. 6, pp. 731-738, 2020. [[CrossRef](#)] [[Google Scholar](#)] [[Publisher Link](#)]
- [29] Bayan Hussein, Nima Abdi, and Ahmed Massoud, "Development of a Three-Phase Interleaved Converter Based on SEPIC DC-DC Converter Operating in Discontinuous Conduction Mode for Ultra-Fast Electric Vehicle Charging Stations," *IET Power Electronics*, vol. 14, no. 11, pp. 1889-1903, 2021. [[CrossRef](#)] [[Google Scholar](#)] [[Publisher Link](#)]
- [30] Anju K. Vincent, and Ruban Nersisson, "Particle Swarm Optimization Based PID Controller Tuning for Level Control of Two Tank System," *IOP Conference Series: Materials Science and Engineering*, vol. 263, pp. 1-7, 2017. [[CrossRef](#)] [[Google Scholar](#)] [[Publisher Link](#)]
- [31] Ahmed M. Mosaad, Mahmoud A. Attia, and Almoataz Y. Abdelaziz, "Whale Optimization Algorithm to Tune PID and PIDA Controllers on AVR System," *Ain Shams Engineering Journal*, vol. 10, no. 4, pp. 755-767, 2019. [[CrossRef](#)] [[Google Scholar](#)] [[Publisher Link](#)]